Acta Cryst E CRYSTALLOGRAPHIC COMMUNICATIONS

ISSN 2056-9890

Synthesis, crystal structure, and Hirshfeld surface analysis of bis{2-[(*E*)-(*p*-tolylimino)methyl]benzen-1-olato}palladium

Nur Nabihah Muzammil,[a] Siti Syaida Sirat,[a,b] Mohd Mustaqim Rosli,[c] Muhamad Azwan Hamali,[a] Mohd Tajudin Mohd Ali[a] and Amalina Mohd Tajuddin[a,b]*

[a]Faculty of Applied Sciences, Universiti Teknologi MARA, Shah Alam, 40450 Shah, Alam, Selangor, Malaysia, [b]Atta-ur-Rahman Institute for Natural Product Discovery (AuRIns), UiTM Puncak, Alam, 42300, Bandar Puncak Alam, Selangor, Malaysia, and [c]X-ray Crystallography Unit, School of Physics, Universiti Sains Malaysia, 11800, USM, Penang, Malaysia. *Correspondence e-mail: amalina9487@uitm.edu.my

Received 30 October 2025
Accepted 23 December 2025

Edited by L. Suescun, Universidad de la República, Uruguay

Keywords: crystal structure; Schiff base; Pd^{II} complex; Hirshfeld surface analysis.

CCDC reference: 2286186

Supporting information: this article has supporting information at journals.iucr.org/e

The title compound, $[Pd(C_{14}H_{12}NO)_2]$, contains an *N,O*-bidentate ligand and features a square-planar Pd^{II} atom coordinated to two chelating ligands. Each ligand binds through one nitrogen atom and one oxygen donor atom, forming two six-membered chelate rings. The Pd^{II} atom lies essentially within the coordination plane, with the *trans* arrangement of the donor atoms giving rise to the square-planar geometry. In the crystal, the molecules are linked through weak C—H···π interactions, which direct the molecular packing. To gain further insights into the intermolecular contacts, a Hirshfeld surface analysis was performed.

1. Chemical context

The coordination chemistry of palladium(II) Schiff base complexes has been explored extensively due to their versatile structural motifs and wide ranging applications in catalysis, bioinorganic chemistry, and materials science (Kargar *et al.*, 2021). Schiff bases derived from aromatic aldehydes and amines, particularly those incorporating salicylaldehyde, have attracted significant attention in structural studies (Aggoun *et al.*, 2020). Among these, ligands formed by the condensation of salicylaldehyde with substituted anilines are known to stabilize square-planar Pd^{II} atoms while enabling systematic tuning of electronic and steric properties (El-Qisairi *et al.*, 2023). Numerous Pd^{II}–Schiff base complexes bearing *N,O*-bidentate chelating ligands have been synthesized and structurally characterized, highlighting variations in Pd—N and Pd—O bond lengths reflecting the influence of ligand substituents (Celedón *et al.*, 2020; El-Qisairi *et al.*, 2023; Khanmoradi *et al.*, 2017).

Reports of palladium(II) complexes with salicylidene-*para*-toluidine derivatives are less frequent than those with unsubstituted salicylideneanilines. The incorporation of a *para*-methyl substituent into the aniline fragment can modify both the steric and electronic environments around the metal center, thereby influencing intermolecular interactions and supramolecular assembly in the solid state (Tudu *et al.*, 2024).

Herein, we report the synthesis of a Schiff base ligand obtained by the condensation of salicylaldehyde with *para*-toluidine, and its coordination to palladium(II) to yield a square-planar complex, $C_{28}H_{24}N_2O_2Pd$, **1**. The Schiff base ligand has been reported previously; however, complex **1**

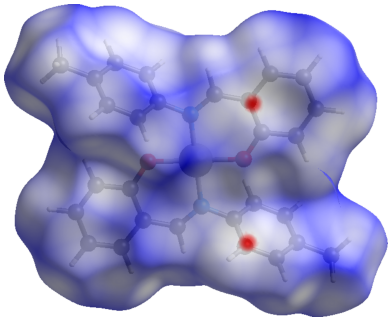

described in this work is new. It was characterized using solid-state analysis such as melting point, elemental analysis and IR spectroscopy, as presented in the experimental section. The single crystals suitable for X-ray diffraction were grown from the filtrate of the crude product; however, the amount obtained was insufficient for elemental analysis. Nevertheless, the pure crystalline product is expected to have the same elemental (C, H, N) composition as the analyzed crude sample, with only minor deviations (Tsionou *et al.*, 2017). Single-crystal X-ray diffraction and Hirshfeld surface analysis were employed to elucidate the influence of the *para*-methyl substituent on the structural parameters and intermolecular interactions in this class of palladium(II) Schiff base derivatives.

In addition to the solid-state analyses, **1** was also fully characterized in solution using NMR and UV-Vis (see supporting information). These techniques provide additional evidence for successful complex formation and, importantly, indicate that the molecular structure observed in the solid state is largely preserved in solution. The ^{1}H and ^{13}C NMR spectra showed the expected ligand coordination shifts, confirming that no structural rearrangement occurs upon dissolution in $CDCl_3$. Furthermore, the solubility of **1** in this non-polar solvent is consistent with the Hirshfeld surface analysis, which revealed relatively weak intermolecular interactions in the crystal packing (Hangan *et al.*, 2023). This correlation between solid-state interactions and solution behavior enhances our understanding of the structural stability of **1**.

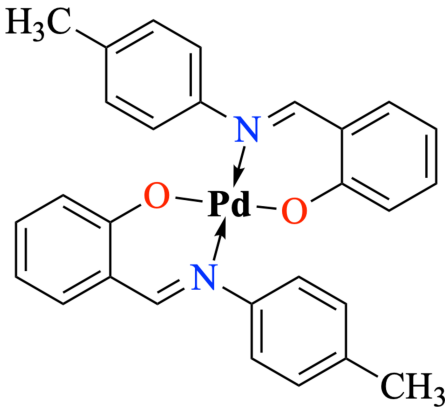

2. Structural commentary

The molecular structure of **1** is shown in Fig. 1. It shows a crystallographically imposed centre of symmetry, with the Pd^{II} atom lying on an inversion center. The Pd^{II} atom adopts a square-planar geometry, being chelated by two *N,O*-bidentate ligands, $C_{14}H_{13}NO$, each chelating through one nitrogen atom and one oxygen donor atom. The two benzene rings, C1–C6 and C8–C13, are planar with maximum deviations of 0.009 (5) and 0.008 (3) for atoms C5 and C8, respectively, from their mean square planes. The dihedral angle between the rings is 52.0 (2)°. All observed bond lengths and angles involving Pd and the ligand (Table 1) fall within the values expected from compounds previously reported by our team (Rosnizam *et al.*, 2022; Ahmad *et al.*, 2020; Mohd Tajuddin *et al.*, 2015).

Table 1
Selected bond lengths (Å) and bond angles (°) in **1**.

Bond lengths (Å)		Bond angles (°)	
Pd1—O1	1.969 (3)	Pd1—O1—C1	125.4 (2)
O1—C1	1.316 (5)	N2—Pd1—O1	91.41 (11)
Pd1—N2	2.023 (3)	Pd1—N2—C7	123.4 (2)
N2—C7	1.290 (4)	Pd1—N2—C8	120.0 (2)
N2—C8	1.443 (5)		

Table 2
C—H···π interaction (Å, °).

D—H···*A*	*D*—H, π	H···*A*	*D*···*A*	*D*—H···*A*
C11—H11···*Cg*3^{i}	34	2.81	3.542 (5)	136

Symmetry code: (i) $x, \frac{3}{2} - y, \frac{1}{2} + z$. *Cg*3 is the centroid of the C1–C6 ring.

3. Supramolecular features

In the crystal, the molecules pack in a three-dimensional arrangement without the formation of intermolecular hydrogen bonds or π–π stacking interactions. Adjacent molecules are not parallel and adopt different orientations within the crystal structure. Fig. 2 shows the molecular packing viewed along the *b*-axis direction. The only interaction between molecules is a weak C—H···π contact between C11—H11 and the centroid of the C1–C6 ring *Cg*3 (Table 2).

There is a short contact between Pd1 and H5 in the crystal structure, which is appeared in the Hirshfeld surface fingerprint plots. However, H5 is a hydrogen atom attached to carbon, positioned geometrically rather than found in the difference-Fourier map. Therefore, this contact should not be interpreted as a significant Pd···H interaction.

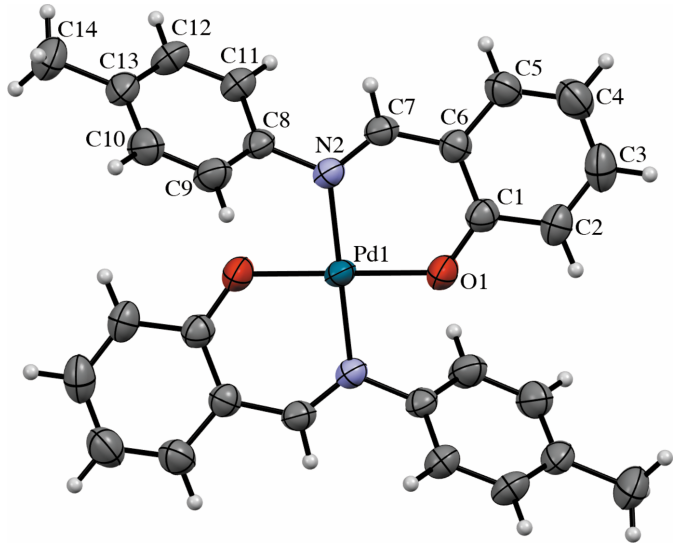

Figure 1
The molecular structure of **1**, showing 50% probability displacement ellipsoids and the atom-numbering scheme. Unlabelled atoms are generated by the symmetry operation ($-x, -y, -z$).

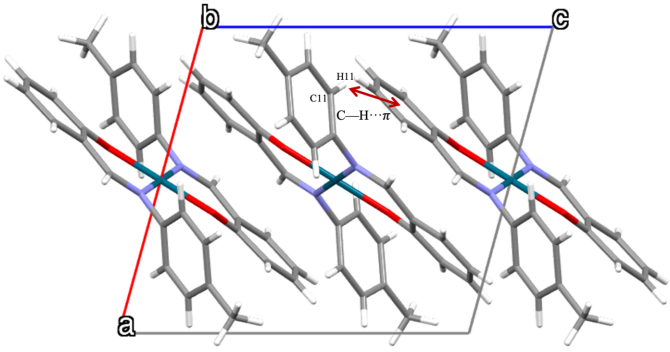

Figure 2
The crystal packing of **1**, viewed along *b*-axis.

4. Hirshfeld surface analysis

A Hirshfeld surface analysis was carried out to investigate and visualize the intermolecular interactions present between molecules and, importantly, to quantify the individual contributions of these contacts to the overall packing (Gannouni *et al.*, 2023). The Hirshfeld surface was generated using *CrystalExplorer 21.5* (Fig. 3). Consistent with the crystallographic analysis, no strong hydrogen-bond interactions are observed in **1**. Instead, the Hirshfeld surface mapped over the d_{norm} displays several small bright-red spots, corresponding to weak and longer range interactions that contribute to the consolidation of the packing.

In addition, shape-index and curvedness surface analyses were performed to predict the existence of C—H···π interactions, as shown in Fig. 4*a* and *b*, respectively. The C—H···π interaction is indicated by the bright-orange concave region marked by black arrows (Luo *et al.*, 2014) while large flat regions are shown by a blue outline on the curvedness diagram.

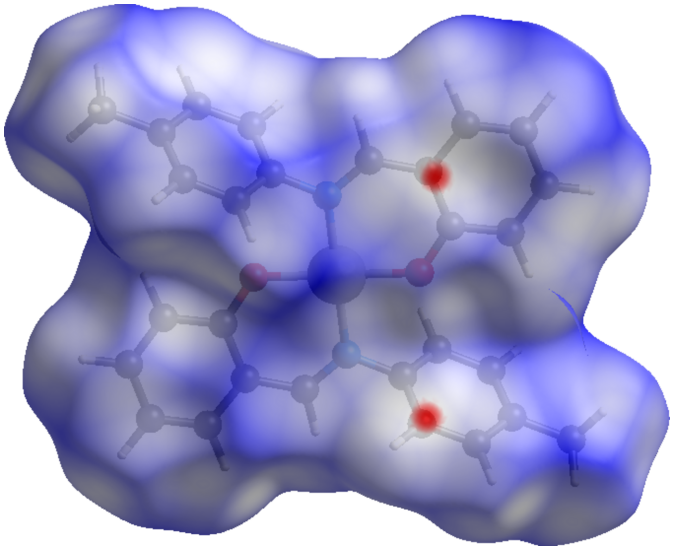

Figure 3
Hirshfeld surface of **1**, mapped over d_{norm}.

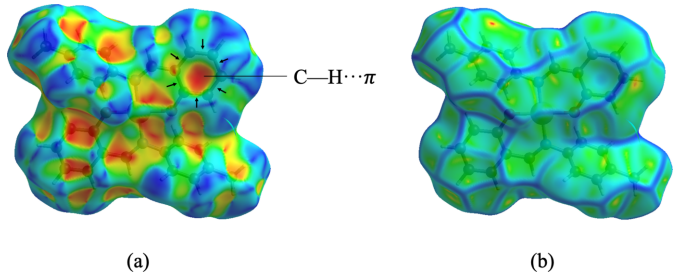

Figure 4
Hirshfeld surface of **1** plotted over (*a*) shape-index and (*b*) curvedness.

The percentage contributions of the intermolecular interactions to the total Hirshfeld surface were quantified by two-dimensional fingerprint plots (Suda *et al.*, 2023). The fingerprint plots of d_i *versus* d_e shown in Fig. 5 reveal that the most significant contributions arise from H···H (57.4%) and C···H/H···C (29.3%) contacts. The wing-like features in the C···H/H···C plot is another indication of the presence of C—H···π interactions (Spackman & McKinnon, 2002). Smaller contributions are observed for O···H/H···O (5.4%), C···C (3.0%), N···H/H···N (2.3%), Pd···H/H···Pd (2.2%), and C···N/N···C (0.4%) interactions. Here, the d_i corresponds to the closest internal distance from a given point on the Hirshfeld surface, while d_e represents the closest external distance to neighboring molecules.

5. Database survey

A search of the Cambridge Structural Database (webCSD accessed October 2025; Groom *et al.*, 2016) for **1** returned no relevant hits. However, a search with generalized bidentate *N, O*-chelating Schiff base palladium(II) complexes with similar structures returned a number of hits including CSD refcodes COZHAA (Manotti Lanfredi *et al.*, 1985), GATBOT (Lai *et al.*, 2005), NENJAR (Zhou *et al.*, 2000), XEKXUJ (Saxena & Murugavel, 2017) and XOJHOW (Kassim *et al.*, 2019). Although JUPWAW (Moreno-Narváez *et al.*, 2025) features a very similar molecular framework, its packing arrangement differs significantly from **1**. These differences mainly arise from substituent effects, particularly the CF_3 group, which modifies the intermolecular contacts and weakens the π–π stacking. A similar behavior is seen in KIKZOX (Waziri *et al.*,

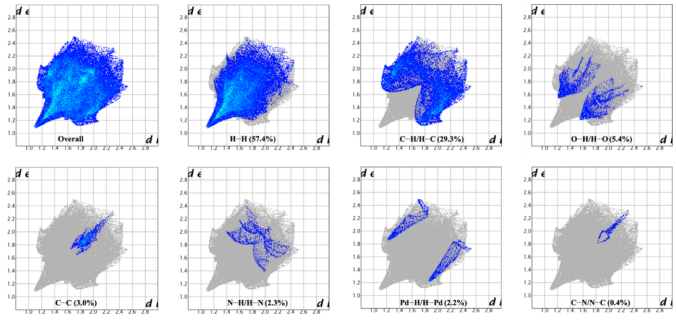

Figure 5
Two-dimensional fingerprint plots for **1**.

Table 3
Experimental details.

Crystal data	
Chemical formula	$[Pd(C_{14}H_{12}NO)_2]$
M_r	526.89
Crystal system, space group	Monoclinic, $P2_1/c$
Temperature (K)	299
a, b, c (Å)	9.941 (3), 10.952 (3), 10.969 (3)
β (°)	105.337 (8)
V (Å^3)	1151.8 (5)
Z	2
Radiation type	Mo $K\alpha$
μ (mm^{-1})	0.83
Crystal size (mm)	0.27 × 0.23 × 0.17
Data collection	
Diffractometer	Bruker APEXII CCD
Absorption correction	Multi-scan (*SADABS*; Krause *et al.*, 2015)
T_{min}, T_{max}	0.640, 0.746
No. of measured, independent and observed [$I > 2\sigma(I)$] reflections	28335, 2866, 2202
R_{int}	0.041
(sin $\theta/\lambda)_{max}$ (Å^{-1})	0.667
Refinement	
$R[F^2 > 2\sigma(F^2)]$, $wR(F^2)$, S	0.043, 0.102, 1.26
No. of reflections	2866
No. of parameters	152
H-atom treatment	H-atom parameters constrained
$\Delta\rho_{max}$, $\Delta\rho_{min}$ (e Å^{-3})	0.86, −0.59

Computer programs: *APEX2* and *SAINT* (Bruker, 2014), *SHELXTL* (Sheldrick, 2015*a*), *SHELXL2014/7* (Sheldrick, 2015*b*) and *OLEX2* (Dolomanov *et al.*, 2009).

2023) and XIVGOC (Meena *et al.*, 2023), where changes in the aromatic rings with different substituents lead to different packing arrangements. This shows that even small substituent changes can significantly affect the overall crystal packing.

6. Synthesis and crystallization

The free ligand [CCDC No. 1470130 (Mague & Mohamed, 2016); 2.113 g, 10 mmol] was dissolved in hot ethanol in a 100 mL round-bottom flask. Palladium(II) acetate (1.123 g, 5 mmol) was dissolved separately in hot ethanol and added into the flask containing the ligand solution. The mixture was stirred and refluxed for 6 h, affording a brown solid. The solid was collected by filtration, washed with ice-cold ethanol, and air-dried at room temperature. Recrystallization by slow evaporation from chloroform at room temperature yielded orange block crystals of **1**. Yield 92.4%, m.p. 594–595 K. Elemental analysis for $C_{28}H_{24}N_2O_4Pd$ calculated (obtained): C, 63.82 (62.94); H, 4.59 (4.48); N, 5.32 (5.17). UV-Vis (acetonitrile, nm) λ_{max}, 247 [π–π^* (C═C)], 295 [π–π^* (C═N)], 416 (n–π^*), 508 (LMCT). IR (KBr, cm^{-1}): 1597 ν(C═N), 1381 ν(C—N), 1314 ν(C—O), 542 ν(Pd—N), 449 ν(Pd—O). ^{1}H NMR (500 MHz, $CDCl_3$) δ ppm: 2.45 [*s*, 3H, C^{11}—H (Ar)], 6.17–6.20 [*m*, 4H, C^{9,10}—H (Ar)], 6.50–6.55 [*m*, 1H, C^4—H (Ar)], 7.11–7.12 [*m*, 1H, C^5—H (Ar)], 7.14–7.16 [*m*, 1H, C^3—H (Ar)], 7.18–7.19 [*m*, 1H, C^2—H (Ar)], 7.73 (*s*, 1H, HC^7═N). ^{13}C NMR (500 MHz, $CDCl_3$) δ ppm: 30.9 (C^{12}), 115.1 [C^2 (Ar)], 120.3 [C^6 (Ar)], 120.7 [C^4 (Ar)], 124.4 [C^9—H (Ar)], 128.6 [C^{10} (Ar)], 134.4 [C^5 (Ar)], 135.0 [C^3 (Ar)], 136.1 [C^{11} (Ar)], 147.1 [C^8 (Ar)], 162.7 (C^7═N), 165.2 (C^1).

7. Refinement

Crystal data, data collection and structure refinement details are summarized in Table 3. H atoms were positioned geometrically (0.93–0.96 Å) and refined as riding with U_{iso}(H) = 1.2–1.5U_{eq}(C).

Acknowledgements

The authors would like to acknowledge Faculty of Applied Sciences and Atta-ur-Rahman Institute for Natural Product Discovery (AuRIns), Universiti Teknologi MARA for the facilities. The authors would also like to express appreciation to Universiti Teknologi MARA (UiTM) for research grant No. 600-RMC/GIP 5/3 (026/2024) and the Ministry of Higher Education (MoHE) for the MyBrainSc scholarship.

Funding information

Funding for this research was provided by: Universiti Teknologi MARA, Institute of Research Management and Innovation, Universiti Teknologi MARA (Grant No. 600-RMC/GIP 5/3 (026/2024) to Amalina Mohd Tajuddin).

References

Aggoun, D., Fernández-García, M., López, D., Bouzerafa, B., Ouennoughi, Y., Setifi, F. & Ourari, A. (2020). *Polyhedron* **187**, 114640.
Ahmad, N., Anouar, E. H., Tajuddin, A. M., Ramasamy, K., Yamin, B. M. & Bahron, H. (2020). *PLoS One* **15**, 0231147. https://doi.org/10.1371/journal.pone.0231147
Bruker (2014). *APEX2* and *SAINT*. Bruker AXS Inc., Madison, Wisconsin, USA.
Celedón, S., Roisnel, T., Artigas, V., Fuentealba, M., Carrillo, D., Ledoux-Rak, I., Hamon, J. & Manzur, C. (2020). *New J. Chem.* **44**, 9190–9201.
Dolomanov, O. V., Bourhis, L. J., Gildea, R. J., Howard, J. A. K. & Puschmann, H. (2009). *J. Appl. Cryst.* **42**, 339–341.
El-Qisairi, A. K., Qaseer, H. A. & Al-Btoush, W. (2023). *Jordan J. Chem.* **18**, 43–52. https://doi.org/10.47014/18.1.5
Gannouni, A., Tahri, W., Roisnel, T., Al-Resayes, S. I., Azam, M. & Kefi, R. (2023). *ACS Omega* **8**, 7738–7748.
Groom, C. R., Bruno, I. J., Lightfoot, M. P. & Ward, S. C. (2016). *Acta Cryst.* B**72**, 171–179.
Hangan, A. C., Lucaciu, R. L., Turza, A., Dican, L., Sevastre, B., Páll, E., Oprean, L. S. & Borodi, G. (2023). *Int. J. Mol. Sci.* **24**, 13819.
Kargar, H., Ardakani, A. A., Tahir, M. N., Ashfaq, M. & Munawar, K. S. (2021). *J. Mol. Struct.* **1233**, 1–12.
Kassim, K., Kahar, M. A. M., Yamin, B. M., Manan, M. A. F. A. & Yusof, M. S. M. (2019). *X-ray Struct. Anal. Online* **35**, 25–26.
Khanmoradi, M., Nikoorazm, M. & Ghorbani-Choghamarani, A. (2017). *Catal. Lett.* **147**, 1114–1126.
Krause, L., Herbst-Irmer, R., Sheldrick, G. M. & Stalke, D. (2015). *J. Appl. Cryst.* **48**, 3–10.
Lai, Y. C., Chen, H. Y., Hung, W. C., Lin, C. C. & Hong, F. E. (2005). *Tetrahedron* **61**, 9484–9489.
Luo, Y. H., Mao, Q. X. & Sun, B. W. (2014). *Inorg. Chim. Acta* **412**, 60–66.
Mague, J. T. & Mohamed, S. K. (2016). *CSD Communication* (refcode CULPOO02). CCDC, Cambridge, England.
Manotti Lanfredi, A. M., Ugozzoli, F., Ghedini, M. & Licoccia, S. (1985). *Acta Cryst.* C**41**, 192–194.
Meena, D. R., Meena, S. & Singh, S. (2023). *Polyhedron* **245**, 116655.

Mohd Tajuddin, A., Bahron, H., Mohd Zaki, H., Kassim, K. & Chantrapromma, S. (2015). *Acta Cryst.* E**71**, 350–353.
Moreno-Narváez, M. E., Arenaza-Corona, A., González-Sebastián, L., Ramírez, T. A., Ortega, S. H., Cruz-Navarro, J. A., Alí-Torres, J., Orjuela, A. L., Reyes-Marquez, V., Lomas-Romero, L. & Morales-Morales, D. (2025). *New J. Chem.* **49**, 5187–5199.
Rosnizam, A. R., Hamali, M. A., Muhammad Low, A. L., Anouar, E. H., Youssef, H. M., Bahron, H. & Mohd Tajuddin, A. (2022). *J. Mol. Struct.* **1260**, 132821.
Saxena, P. & Murugavel, R. (2017). *ChemistrySelect* **2**, 3812–3822.
Sheldrick, G. M. (2015*a*). *Acta Cryst.* A**71**, 3–8.
Sheldrick, G. M. (2015*b*). *Acta Cryst.* C**71**, 3–8.
Spackman, M. A. & McKinnon, J. J. (2002). *CrystEngComm* **4**, 378–392.
Suda, S., Tateno, A., Nakane, D. & Akitsu, T. (2023). *Int. J. Org. Chem.* **13**, 57–85.
Tsionou, M. I., Knapp, C. E., Foley, C. A., Munteanu, C. R., Cakebread, A., Imberti, C., Eykyn, T. R., Young, J. D., Paterson, B. M., Blower, J. & Ma, M. T. (2017). *RSC Adv.* **7**, 49586–49599.
Tudu, P., Dan, S. & Chowdhury, P. (2024). *J. Res. Chem.* **5**, 36–39.
Waziri, I., Yusuf, T. L., Zarma, H. A., Oselusi, S. O., Coetzee, L. C. C. & Adeyinka, A. S. (2023). *Inorg. Chim. Acta* **552**, 121505.
Zhou, X. G., Huang, J. S., Yu, X. Q., Zhou, Z. Y. & Che, C. M. (2000). *J. Chem. Soc. Dalton Trans.* pp. 1075–1080.

supporting information

Acta Cryst. (2026). E**82**, 138-142 [https://doi.org/10.1107/S2056989025011570]

Synthesis, crystal structure, and Hirshfeld surface analysis of bis{2-[(*E*)-(*p*-tolylimino)methyl]benzen-1-olato}palladium

Nur Nabihah Muzammil, Siti Syaida Sirat, Mohd Mustaqim Rosli, Muhamad Azwan Hamali, Mohd Tajudin Mohd Ali and Amalina Mohd Tajuddin

Computing details

Bis{2-[(*E*)-(*p*-tolylimino)methyl]benzen-1-olato}palladium

Crystal data

$[Pd(C_{14}H_{12}NO)_2]$
$M_r = 526.89$
Monoclinic, $P2_1/c$
$a = 9.941$ (3) Å
$b = 10.952$ (3) Å
$c = 10.969$ (3) Å
$\beta = 105.337$ (8)°
$V = 1151.8$ (5) Å^3
$Z = 2$
$F(000) = 536$
$D_x = 1.519$ Mg m^{-3}
Mo $K\alpha$ radiation, $\lambda = 0.71073$ Å
Cell parameters from 8213 reflections
$\theta = 2.7$–$28.3°$
$\mu = 0.83$ mm^{-1}
$T = 299$ K
Block, orange
0.27 × 0.23 × 0.17 mm

Data collection

Bruker APEXII CCD diffractometer
φ and ω scans
Absorption correction: multi-scan (SADABS; Krause *et al.*, 2015)
$T_{min} = 0.640$, $T_{max} = 0.746$
28335 measured reflections
2866 independent reflections
2202 reflections with $I > 2\sigma(I)$
$R_{int} = 0.041$
$\theta_{max} = 28.3°$, $\theta_{min} = 3.7°$
$h = -13 \rightarrow 13$
$k = -14 \rightarrow 14$
$l = -14 \rightarrow 14$

Refinement

Refinement on F^2
Least-squares matrix: full
$R[F^2 > 2\sigma(F^2)] = 0.043$
$wR(F^2) = 0.102$
$S = 1.26$
2866 reflections
152 parameters
0 restraints
Hydrogen site location: inferred from neighbouring sites
H-atom parameters constrained
$w = 1/[\sigma^2(F_o^2) + 2.4894P]$ where $P = (F_o^2 + 2F_c^2)/3$
$(\Delta/\sigma)_{max} < 0.001$
$\Delta\rho_{max} = 0.86$ e Å^{-3}
$\Delta\rho_{min} = -0.59$ e Å^{-3}

Special details

Geometry. All esds (except the esd in the dihedral angle between two l.s. planes) are estimated using the full covariance matrix. The cell esds are taken into account individually in the estimation of esds in distances, angles and torsion angles; correlations between esds in cell parameters are only used when they are defined by crystal symmetry. An approximate (isotropic) treatment of cell esds is used for estimating esds involving l.s. planes.

Fractional atomic coordinates and isotropic or equivalent isotropic displacement parameters (Å²)

	x	*y*	*z*	U_{iso}*/U_{eq}
Pd1	0.500000	0.500000	0.500000	0.03766 (12)
O1	0.3935 (3)	0.4667 (3)	0.3246 (2)	0.0581 (7)
N2	0.5448 (3)	0.6713 (2)	0.4539 (3)	0.0392 (6)
C1	0.3344 (4)	0.5497 (3)	0.2408 (3)	0.0428 (7)
C2	0.2337 (4)	0.5091 (4)	0.1321 (4)	0.0515 (9)
H2	0.208633	0.427112	0.123439	0.062*
C3	0.1729 (5)	0.5909 (5)	0.0392 (4)	0.0630 (12)
H3	0.104590	0.563363	−0.030722	0.076*
C4	0.2103 (5)	0.7145 (5)	0.0461 (4)	0.0646 (12)
H4	0.168698	0.768064	−0.018704	0.078*
C5	0.3086 (4)	0.7546 (4)	0.1495 (4)	0.0544 (9)
H5	0.334922	0.836317	0.154478	0.065*
C6	0.3715 (4)	0.6750 (3)	0.2496 (3)	0.0413 (7)
C7	0.4794 (4)	0.7252 (3)	0.3506 (3)	0.0415 (7)
H7	0.505099	0.805438	0.340683	0.050*
C8	0.6467 (4)	0.7435 (3)	0.5430 (3)	0.0385 (7)
C9	0.7833 (4)	0.7047 (4)	0.5833 (4)	0.0537 (9)
H9	0.810674	0.632149	0.552762	0.064*
C10	0.8788 (4)	0.7742 (4)	0.6691 (4)	0.0570 (10)
H10	0.971174	0.748409	0.694419	0.068*
C11	0.6069 (4)	0.8514 (3)	0.5879 (3)	0.0432 (8)
H11	0.515493	0.878994	0.559108	0.052*
C12	0.7042 (4)	0.9185 (3)	0.6764 (4)	0.0515 (9)
H12	0.676592	0.990310	0.708025	0.062*
C13	0.8418 (4)	0.8808 (3)	0.7188 (4)	0.0493 (9)
C14	0.9460 (5)	0.9557 (5)	0.8140 (5)	0.0717 (13)
H14A	0.908489	1.035761	0.819350	0.108*
H14B	1.030731	0.962422	0.788258	0.108*
H14C	0.965089	0.916874	0.895262	0.108*

Atomic displacement parameters (Å²)

	U^{11}	U^{22}	U^{33}	U^{12}	U^{13}	U^{23}
Pd1	0.0499 (2)	0.02614 (17)	0.03647 (19)	−0.00358 (14)	0.01066 (15)	−0.00313 (13)
O1	0.081 (2)	0.0433 (14)	0.0403 (14)	−0.0127 (14)	−0.0009 (13)	−0.0049 (11)
N2	0.0454 (15)	0.0315 (13)	0.0402 (14)	−0.0016 (11)	0.0102 (12)	−0.0040 (11)
C1	0.0488 (19)	0.0414 (18)	0.0391 (17)	−0.0018 (15)	0.0132 (15)	−0.0034 (14)
C2	0.053 (2)	0.058 (2)	0.0423 (19)	−0.0057 (18)	0.0097 (16)	−0.0121 (17)
C3	0.054 (2)	0.087 (3)	0.042 (2)	0.003 (2)	0.0022 (18)	−0.013 (2)

C4	0.067 (3)	0.067 (3)	0.054 (2)	0.017 (2)	0.005 (2)	0.005 (2)
C5	0.061 (2)	0.049 (2)	0.051 (2)	0.0110 (18)	0.0102 (18)	0.0020 (17)
C6	0.0460 (18)	0.0410 (18)	0.0377 (17)	0.0018 (14)	0.0123 (14)	−0.0023 (14)
C7	0.0488 (19)	0.0320 (16)	0.0446 (18)	−0.0010 (14)	0.0139 (15)	−0.0008 (14)
C8	0.0431 (17)	0.0318 (15)	0.0405 (17)	−0.0058 (13)	0.0108 (14)	−0.0006 (13)
C9	0.049 (2)	0.0386 (19)	0.070 (3)	0.0025 (16)	0.0101 (19)	−0.0075 (18)
C10	0.045 (2)	0.051 (2)	0.068 (3)	−0.0005 (17)	0.0040 (19)	0.0013 (19)
C11	0.0460 (19)	0.0380 (17)	0.0467 (19)	−0.0040 (14)	0.0142 (15)	−0.0061 (14)
C12	0.061 (2)	0.0366 (18)	0.057 (2)	−0.0044 (17)	0.0158 (19)	−0.0122 (16)
C13	0.055 (2)	0.0422 (19)	0.047 (2)	−0.0107 (16)	0.0058 (17)	−0.0014 (16)
C14	0.071 (3)	0.067 (3)	0.065 (3)	−0.020 (2)	−0.003 (2)	−0.010 (2)

Geometric parameters (Å, º)

Pd1—O1	1.969 (3)	C6—C7	1.432 (5)
Pd1—O1^{i}	1.969 (3)	C7—H7	0.9300
Pd1—N2^{i}	2.023 (3)	C8—C9	1.380 (5)
Pd1—N2	2.023 (3)	C8—C11	1.378 (5)
O1—C1	1.316 (5)	C9—H9	0.9300
N2—C7	1.290 (4)	C9—C10	1.376 (6)
N2—C8	1.443 (4)	C10—H10	0.9300
C1—C2	1.411 (5)	C10—C13	1.379 (6)
C1—C6	1.418 (5)	C11—H11	0.9300
C2—H2	0.9300	C11—C12	1.386 (5)
C2—C3	1.371 (6)	C12—H12	0.9300
C3—H3	0.9300	C12—C13	1.386 (6)
C3—C4	1.401 (7)	C13—C14	1.505 (5)
C4—H4	0.9300	C14—H14A	0.9600
C4—C5	1.359 (6)	C14—H14B	0.9600
C5—H5	0.9300	C14—H14C	0.9600
C5—C6	1.412 (5)		
O1—Pd1—O1^{i}	180.0	N2—C7—C6	127.2 (3)
O1^{i}—Pd1—N2	88.59 (11)	N2—C7—H7	116.4
O1—Pd1—N2	91.41 (11)	C6—C7—H7	116.4
O1—Pd1—N2^{i}	88.59 (11)	C9—C8—N2	120.2 (3)
O1^{i}—Pd1—N2^{i}	91.41 (11)	C11—C8—N2	119.7 (3)
N2^{i}—Pd1—N2	180.0	C11—C8—C9	120.1 (3)
C1—O1—Pd1	125.4 (2)	C8—C9—H9	120.3
C7—N2—Pd1	123.4 (2)	C10—C9—C8	119.4 (4)
C7—N2—C8	116.4 (3)	C10—C9—H9	120.3
C8—N2—Pd1	120.0 (2)	C9—C10—H10	119.0
O1—C1—C2	117.3 (3)	C9—C10—C13	122.1 (4)
O1—C1—C6	124.1 (3)	C13—C10—H10	119.0
C2—C1—C6	118.4 (3)	C8—C11—H11	120.3
C1—C2—H2	120.1	C8—C11—C12	119.5 (4)
C3—C2—C1	119.8 (4)	C12—C11—H11	120.3
C3—C2—H2	120.1	C11—C12—H12	119.3

C2—C3—H3	118.9	C11—C12—C13	121.4 (3)
C2—C3—C4	122.2 (4)	C13—C12—H12	119.3
C4—C3—H3	118.9	C10—C13—C12	117.5 (3)
C3—C4—H4	120.7	C10—C13—C14	122.0 (4)
C5—C4—C3	118.6 (4)	C12—C13—C14	120.5 (4)
C5—C4—H4	120.7	C13—C14—H14A	109.5
C4—C5—H5	119.3	C13—C14—H14B	109.5
C4—C5—C6	121.5 (4)	C13—C14—H14C	109.5
C6—C5—H5	119.3	H14A—C14—H14B	109.5
C1—C6—C7	123.5 (3)	H14A—C14—H14C	109.5
C5—C6—C1	119.4 (3)	H14B—C14—H14C	109.5
C5—C6—C7	116.9 (3)		

Pd1—O1—C1—C2	−164.1 (3)	C4—C5—C6—C1	1.8 (6)
Pd1—O1—C1—C6	19.8 (5)	C4—C5—C6—C7	176.6 (4)
Pd1—N2—C7—C6	−3.2 (5)	C5—C6—C7—N2	175.7 (4)
Pd1—N2—C8—C9	61.7 (4)	C6—C1—C2—C3	−1.0 (6)
Pd1—N2—C8—C11	−118.1 (3)	C7—N2—C8—C9	−123.2 (4)
O1—C1—C2—C3	−177.4 (4)	C7—N2—C8—C11	56.9 (4)
O1—C1—C6—C5	175.3 (4)	C8—N2—C7—C6	−178.1 (3)
O1—C1—C6—C7	0.8 (6)	C8—C9—C10—C13	1.5 (7)
N2—C8—C9—C10	−179.5 (4)	C8—C11—C12—C13	1.5 (6)
N2—C8—C11—C12	178.0 (3)	C9—C8—C11—C12	−1.8 (5)
C1—C2—C3—C4	2.0 (7)	C9—C10—C13—C12	−1.8 (6)
C1—C6—C7—N2	−9.7 (6)	C9—C10—C13—C14	179.1 (4)
C2—C1—C6—C5	−0.8 (5)	C11—C8—C9—C10	0.4 (6)
C2—C1—C6—C7	−175.3 (3)	C11—C12—C13—C10	0.3 (6)
C2—C3—C4—C5	−1.1 (7)	C11—C12—C13—C14	179.4 (4)
C3—C4—C5—C6	−0.8 (7)		

Symmetry code: (i) −*x*+1, −*y*+1, −*z*+1.